ASCE

Fracture and Size Effect Suppression by Mesh Reinforcement of Concrete and Justification of Empirical Shrinkage and Temperature Reinforcement in Design Codes

Mohammad Rasoolinejad[1]; A. Abdullah Dönmez[2]; and Zdeněk P. Bažant, Hon.M.ASCE[3]

Abstract: A minimum mesh reinforcement, called the shrinkage and temperature reinforcement, has been required by ACI design code for 92 years to attain ductility with no formation of large localized cracks. The required steel ratio, which is 0.18%, has been empirical. In this paper, it is shown that it can be explained theoretically and justified approximately by finite-element analysis of the size effect and crack growth based on quasibrittle fracture mechanics, in which the microplane model M7 and crack band model are used. The premise, which simplifies the analysis, is that the cracking would localize into wider cracks if and only if there is a size effect. The size effect can be completely avoided only if, for the same cross-section area, the tensile strength of yielding reinforcement is greater that the tensile strength of concrete. The effect of increasing the reinforcement ratio is also explored. The calculations indicate that fracture mechanics can, and should, be used to check ductility and size effect implications in the two-sided reinforced members, boundary beams, and more complicated designs such as in shear walls. **DOI: 10.1061/(ASCE)EM.1943-7889.0001850.**

Author keywords: Reinforced concrete; Minimum reinforcement; Scaling; Quasibrittle fracture; Finite-element analysis; Ductility; Brittleness; Postpeak softening; Structural design.

Introduction

Since 1928, the American Concrete Institute design code ACI 318 has required a minimum reinforcement for concrete slabs and walls (Suprenant 2002). It is called the shrinkage and temperature reinforcement and consists of a rectangular mesh of reinforcing steel bars. According to the current code [ACI 318-2019 (ACI 2019)], the steel ratio, ρ, must be at least 0.18% for each of two orthogonal directions. In the previous code version, it was 0.20% for Grade 40 or 50 deformed bars, and 0.18% (or $60{,}000/f_y$) for yield stress $f_y > 60{,}000$ psi (1 psi = 6,895 Pa). This reinforcement limit, which has been empirical, approximately ensures that the in-plane tensile stress caused by restraints under nonuniform early shrinkage and thermal strain causes only fine distributed cracking but no localized cracks wide enough for endangering durability (Sule and Van Breugel 2004; Gilbert 1992; Mertol et al. 2010; Kianoush et al. 2008; England and Ross 1962; Wei et al. 2017). For modern concretes, one must also consider the autogenous shrinkage, for which an accurate prediction formula has recently been developed (Rasoolinejad et al. 2019).

The purpose of this study is to explain and justify this requirement by quasibrittle fracture mechanics. Such an explanation then provides credence of applying fracture mechanics to ensure non-localized distributed cracks in various more complicated situations, such as slabs or shear walls with various boundary conditions or with widely separated strong steel bars. Useful studies of the minimum reinforcement have been presented by many authors (Appendix I). None of them, however, approached the subject from the viewpoint of quasibrittle fracture mechanics and its size effect.

The shrinkage and temperature reinforcement, or generally the minimum reinforcement of a slab or wall under tension, has the purpose of limiting the maximum crack width w_c. Localized cracks wider than about 0.5 mm significantly enhance permeability to various corrosive agents. However, as shown by Bažant et al. (1987), hairline cracks of width 0.1 mm (or even 0.2 mm) do not significantly inhibit flow along the crack because the contiguity of the space within the crack is rather limited due to blockage by surface roughness. There are two possible alternatives to ensuring, by calculations, such a negligible crack width:

- Estimate by fracture mechanics the opening width of a possible localized crack. This approach leads to a system of nonlinear algebraic equations.
- Exploit the fact that a mesh-reinforced slab exhibiting a (deterministic) size effect must also exhibit gradual postpeak softening, which in turn leads to localization of distributed fine cracking into fewer and wider cracks.

The former alternative is tedious and only the latter is pursued here. As for size effect tests, no reports are found in the literature (they would be costly, and funding seems unobtainable at present). Nevertheless, the crack band microplane model M7, used here, has been shown in many problems to give results in agreement with experiments. The practical consequence of softening and the localization of distributed cracking into wider cracks is that cracks wider

[1]Postdoctoral Scholar, Northwestern Institute on Complex Systems, 600 Foster St., Evanston, IL 60208. Email: Rasoolinejad@u.northwestern.edu

[2]Postdoctoral Scholar, Dept. of Civil Engineering, İstanbul Teknik Üniversitesi, Istanbul 34469, Turkey. Email: donmezab@itu.edu.tr

[3]McCormick Institute Professor and W. P. Murphy Professor of Civil and Mechanical Engineering and Materials Science, Northwestern Univ., 2145 Sheridan Rd., CEE/A135, Evanston, IL 60208 (corresponding author). Email: z-bazant@northwestern.edu

Note. This manuscript was submitted on January 8, 2020; approved on May 26, 2020; published online on August 11, 2020. Discussion period open until January 11, 2021; separate discussions must be submitted for individual papers. This paper is part of the ***Journal of Engineering Mechanics***, © ASCE, ISSN 0733-9399.

than about 0.3 mm significantly enhance diffusion of moisture with corrosive agents into concrete. However, diffusion analysis, presented by Bažant et al. (1987), is beyond the scope of the present paper.

Size Effect of Mesh-Reinforced Concrete

It is by now well-established that quasibrittle fracture exhibits a strong deterministic size effect. This fact is now recognized in the new design specifications in ACI 318-19 (ACI 2019) by imposing on the concrete shear strength of reinforced beams and slabs the size effect factor $\lambda_s = \min\{[2/(1 + D/D_0)]^{-1/2}, 1\}$ [$D_0 = 25.4$ cm (10 in.)], based on Bažant's size effect law (SEL), Eq. (1). The size effect is a quintessential property of all quasibrittle materials. For concrete, which is archetypical, the fracture size effect has been derived theoretically and amply documented by experiments as well as finite-element (FE) simulations (e.g., Bažant and Le 2017).

According to fracture mechanics, it is not enough to check the crack formation for one slab size. Generally, it is necessary to consider a broad range of sizes and make sure that localized cracks do not propagate for any one of them. To that end, it suffices if the maximum load of a cracked mesh-reinforced concrete slab does not exceed the load at which the bars are yielding.

The simplest way to detect by computer simulations whether distinct localized cracks can propagate through a mesh-reinforced concrete slab is to analyze the size effect in geometrically similar fracture specimens of different sizes D, in which a notch conveniently fixes where the crack would start growing. This study uses standard notched three-point bend beams with a notch that cuts through both the concrete and steel bars and reaches to depth $D/4$, as shown in Fig. 1 (the smallest size). The beams with their notches are geometrically scaled in the ratio 1:8 and their depths are $D = 0.4$, 0.8, 1.6, and 3.2 m.

The reinforcement consists of a square mesh of steel bars with spacing $s = 0.1$ m in both directions. The mesh is considered as a material property (homogenized for the purpose of analysis), and so the bar spacing and diameter are not changed with the beam size (the design code, however, allows increasing bar spacing with slab thickness). According to the crack band model, whose purpose is to avoid spurious mesh sensitivity, the finite-element size h must be treated as a material property related to the fracture energy of material, G_f. Accordingly, either h must be kept constant (in the zone where fracture is expected) or, if h is adjusted, the postpeak softening of constitutive law must be adjusted so as to preserve constant G_f for the crack band. The latter saves computer time, but the former is simpler and more accurate. So, $h = 25$ mm is used in all the present analysis.

The fracture size effect is usually described in terms of the nominal strength of structure, which represents a characteristic

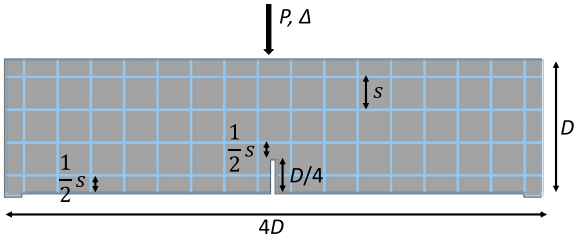

Fig. 1. Specimen geometry. D scales with the size whereas s remains constant for all scales.

of the maximum (or ultimate) load, P, and is defined as $\sigma_N = c_u P/A$, $A = bD$, where D is the characteristic structure size and c_u is a dimensionless factor. For ductile failure of elastoplastic structures, there is no size effect, i.e., σ_N is independent of D. But this is not the case for concrete, as well as fiber composites, tough ceramics, rocks, stiff soils, wood, and sea ice, among others. Such quasibrittle materials can grow long cracks or damage bands in a stable manner before reaching the maximum load. The energy release of such cracks causes an energetic (deterministic) size effect, which is labeled Type 2 and has the following form (Bažant 1984):

$$\sigma_N = \sigma_0 \left(1 + \frac{D}{D_0}\right)^{-1/2} \tag{1}$$

where D = characteristic structure size; σ_0 = ultimate nominal strength of structure for small sizes, for which the plastic limit analysis is applicable; and D_0 = transitional size, which represents the size at the intersection of the small-size strength asymptote and the large-size linear-elastic fracture mechanics (LEFM) asymptote. The Type 2 size effect must be distinguished from Type 1, which has both energetic and statistical causes, is typical of plain concrete, and occurs in (unnotched) structures that fail as soon as a macrocrack begins to propagate from one representative volume element (RVE) in the structure.

Further, it has been shown (Bažant and Kazemi 1990; Bažant and Planas 1997) that

$$\sigma_0 = \sqrt{EG_f/c_f g'(\alpha_0)}, \qquad D_0 = c_f g'(\alpha_0)/g(\alpha_0) \tag{2}$$

where G_f = fracture energy (material constant); E = Young's elastic modulus; $\alpha = a/D$ is the relative (dimensionless) crack length; a = equivalent crack length; $g(\alpha) = K_I^2/\sigma_N^2 D$ is the dimensionless energy release function of LEFM, available in handbooks, where K_I is the stress intensity factor; α_0 = initial value of α for the notch tip; and $c_f = a - a_0$ is the material characteristic length $\approx$ half-size of the fracture process zone (FPZ) (Bažant and Planas 1997).

FE Analysis with M7 and Crack Band Model

The concrete is here characterized by microplane constitutive model M7 (Caner and Bažant 2012a, b), which is the last in a series of progressively improved microplane models (Bažant and Oh 1985; Bažant and Prat 1988). For convenience, a simple explanation and the listing of advantages of this model are given in Appendix II.

As a simple way to avoid spurious mesh sensitivity due to softening cracking damage, the FE analysis based on M7 is conducted with the crack band model (Bažant and Oh 1983). Conceived in 1983, this model is nowadays used in various commercial software (e.g., ATENA, DIANA or, OOFEM and implicitly also in ABAQUS). The correct energy dissipation is ensured by keeping the element size constant (here equal to 25 mm) for all structure sizes. In case the element size would need to be varied (which is not needed here), the postpeak softening slope must be adjusted according to the element size so as to ensure a localized crack band to dissipate the same energy.

The steel is modeled by a simple elastic-plastic constitutive model with no hardening. Young's modulus is 200 GPa, and the yield limit 400 MPa. Various bar diameters are used to represent the variation of the reinforcement ratio ρ, whose values are 0.1%, 0.18%, 0.5%, 1%, 2%, and 5%, the same for both directions. For comparison, plain (or unreinforced) beams are also simulated. The spacing of reinforcing bars is kept constant and is equal to 10 cm for all scales.

Table 1. Default values of the M7 model

Parameter	Value	Meaning
E	25 GPa	Elastic modulus (and vertical scaling parameter)
ν	0.18	Poisson's ratio
k_1	1.5×10^{-4}	Radial scaling parameter
k_2	110	Controls the horizontal asymptote value in the frictional boundary
k_3	30	Controls the shape of the volumetric boundary
k_4	100	Controls the shape of the volumetric boundary
k_5	1×10^{-4}	Controls the volumetric-deviatoric coupling at low pressures

The M7 parameters were calibrated by test data from extensive test data on uniaxial, biaxial, and triaxial compression and tension under proportional and nonproportional loading (Caner and Bažant 2012a). Because no studies of the size effect in mesh-reinforced concrete have been found, the modeling was based on the standard reinforcing steel properties and the concrete predicted by the default parameters of M7 (Caner and Bažant 2012a) corresponding to Young's modulus of 25 GPa and compressive strength 40 MPa (Table 1).

The steel is modeled by truss elements attached at nodes to concrete finite elements, using the Embedded Region feature in ABAQUS version 6.13. This was extensively discussed in the 1970s and 1980s (Shah and Ouyang 1991), and it was concluded that the slip at nodes is important only for local behavior (Bažant and Desmorat 1994). It is unimportant for global behavior such as the size effect, especially for deformed steel bars, and for the opening mode of fracture. The size effect is a global phenomenon, depending on energy release from the whole structure. Commercial FE programs such as ATENA or ABAQUS, which have been well validated, ignore bar slip and, anyway, its proper consideration would introduce major complexity because the slip is a fracture problem whose force-slip relation exhibits postpeak softening with localization instability (Bažant and Desmorat 1994).

The FE mesh for concrete consists of fully integrated hexahedral (C3D8) elements. In the explicit analysis, the mass scaling factor of 4 is used. However, if the kinetic energy exceeds 1% of the strain energy, the analysis is rerun without any mass scaling. To reduce the computational cost, only half of the beam through the thickness simulated, and the boundary condition of symmetry is applied instead. The largest size included 60,000 elements (which required running the computations on the supercomputer cluster Quest of Northwestern University).

FE Fracture Analysis Results

The load-point displacement is incremented up to and beyond the maximum load point. The computed results are presented for various reinforcement ratios ρ and, for comparison, also for plain concrete ($\rho = 0$). The results are plotted in terms of the nominal stress defined as follows:

$$\sigma_N = c_u \frac{P}{bD}; \qquad c_u = \frac{3L}{2D} \tag{3}$$

where P = midspan load; b = beam width; L = beam span; and D = beam depth. Unsurprisingly, the simulations of unreinforced concrete beams [Fig. 2(a)] show a size effect that perfectly follows the size effect law [Fig. 2(b)].

The fracture energy G_f is not used as the direct input of constitutive damage models in general and the microplane model in particular. Rather, the measured size effect in notched fracture specimens is exploited to determine G_f and the characteristic fracture process zone size c_f, and the free parameters of the microplane model are adjusted to match the given G_f. To this end, the Type 2 SEL is related to equivalent LEFM and is obtained from the linear regression plot (Bažant and Kazemi 1990; Bažant and Planas 1997; Bažant and Le 2017)

$$Y = AX + C \tag{4}$$

$$\text{where } X = D; \qquad Y = \frac{1}{\sigma_N^2} \tag{5}$$

$$\text{and} \quad A = \frac{g(\alpha)}{EG_f}; \qquad C = c_f \frac{g'(\alpha)}{EG_f} \tag{6}$$

From the regression plots in Fig. 3, one gets $G_f = 80$ N/m and $c_f = 10.7$ cm (4.25 in.). In theory, a homogenized composite of concrete and reinforcing mesh should also posses its fracture energy, but a simple formula seems impossible because the percentage of yielding steel bars in the damage zone varies (see Appendix III). When the mesh-reinforced concrete is smoothed by a macrocontinuum, its fracture behavior depends, of course, on the bar spacing. The strength contribution of reinforcing mesh, which is superposed on the strength contribution of the fracturing concrete, can be approximately predicted by the plastic limit analysis.

For the case of 0.1% reinforcement, the failure of concrete on the tensile side controls the maximum load. However, as the displacement increases, the load reaches a plateau, which corresponds

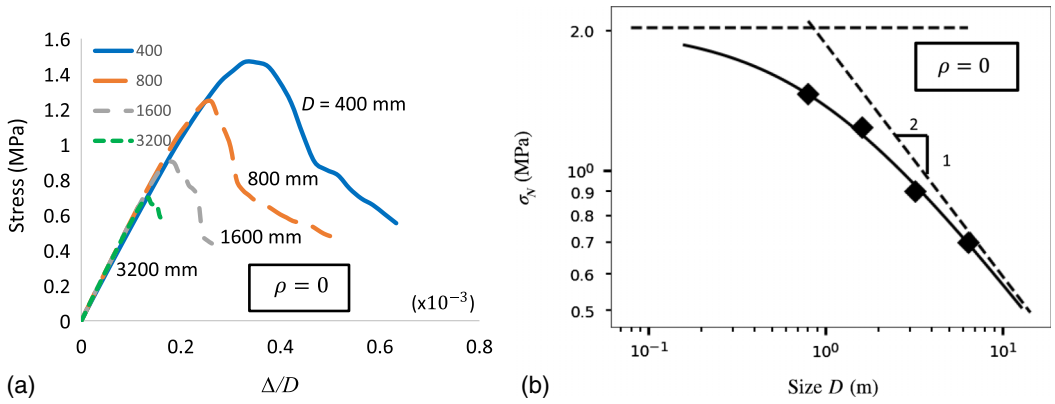

Fig. 2. Simulation results of plain concrete beams: (a) nominal stress versus relative displacement for three-point bend beams; and (b) corresponding double-log size effect plot.

J. Eng. Mech., 2020, 146(10): 04020120

to plastic yield stress in reinforcement [Fig. 4(a)]. Compared with plain concrete, for small sizes, the maximum stress does not change much with the introduction of reinforcement. However, for large sizes, as the stress at concrete failure gets close to the yield limit of reinforcement, the effect of reinforcement on maximum load becomes significant. The size effect curve then deviates from the straight line of LEFM asymptote of slope $-1/2$, and approaches the yield stress value for large sizes (Fig. 5). Upon increasing the reinforcement ratio to 0.18%, the yield plateau almost reaches the tensile strength of the concrete [Fig. 4(b)]. For large sizes, the reinforcement controls the maximum load. For small sizes, the beams with different reinforcement ratios fail at about the same strength (Fig. 5), which indicates the tensile strength in concrete controls the maximum load.

The size effect plot for plain concrete beam ($\rho = 0$) follows, as expected, Bažant's size effect law, Eq. (1). The size effect plot in Fig. 5 for $\rho = 0.1\%$, shows a significantly weaker size effect than for plain concrete. For $\rho = 0.18\%$, the size effect is, as expected, virtually nil (although the homogenized stress in yielding steel approximately equals the strength limit of concrete).

The reinforcement is in full control for $\rho = 0.5$ [Fig. 6(a)], and the peak is no longer governed by concrete. For the largest sizes, one gets softening. That is due to the crushing concrete on the compression side. As observed previously in experiments (Bažant and Ozbolt 1992; Bažant and Cedolin 2010), there is a size effect on the slope of postpeak softening due to concrete crushing; the larger the specimen, the steeper the softening, even though the peak nominal stress does not change. The notched beams with $\rho = 1\%$, 2%, and 5% [Figs. 6(b–d)] show that the postpeak softening due to concrete crushing is getting steeper with increasing ρ as well as with structure size. The steel bars on the compressive side contribute to increasing the compression capacity of the beam and the peak load. The effect of ρ is summarized in Fig. 7.

The simulation results for mesh-reinforced concrete indicate that as the structure size increases, the limit stress of concrete follows the SEL, whereas the stress in yielding bars stays the same. So, for low reinforcement ratios, the size effect emerges as long as the yield limit of bars is less than the failure stress. For medium reinforcement, the steel controls the maximum load, and no size effect is observed. This case occurs when the yield limit of the bars is higher than the tensile strength provided by concrete.

For low reinforcement, with a yield limit less than the tensile strength of concrete at small sizes, the size effect descends from a horizontal asymptote for concrete strength limit at small sizes to a lower asymptote for yield limit at large sizes (Fig. 8). For a strong enough reinforcement, the latter limit becomes higher than the former, and then there is no size effect. A similar horizonal asymptote is observed by the effect of crack-blunting damage (Di Luzio and Cusatis 2018).

Shrinkage and Temperature Reinforcement

The shrinkage and temperature reinforcement ratio of $\rho = 0.18\%$ is required by the current code, ACI 318-2019, for all situations. This is a safe approximation, but the reinforcement ratio and yield limit still have some effect, which is the reason for the discrepancy between the codes of practice (Shehata et al. 2003).

Consider now the steel yield limit to be decreased to 250 MPa and run the computations for the 0.18% case. Fig. 9(a) shows the calculated curve of nominal stress versus deformation. The marked

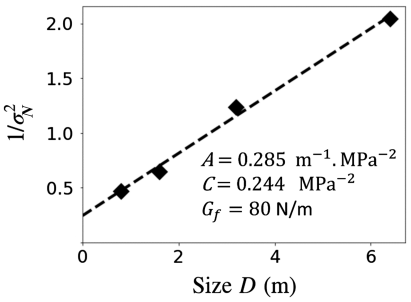

Fig. 3. Linear regression of size effect data yielding fracture energy G_f of plain concrete.

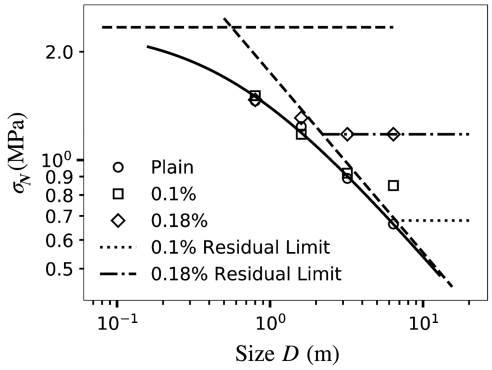

Fig. 5. Double-log size effect plot of the 0.10% and 0.18% reinforcement beams.

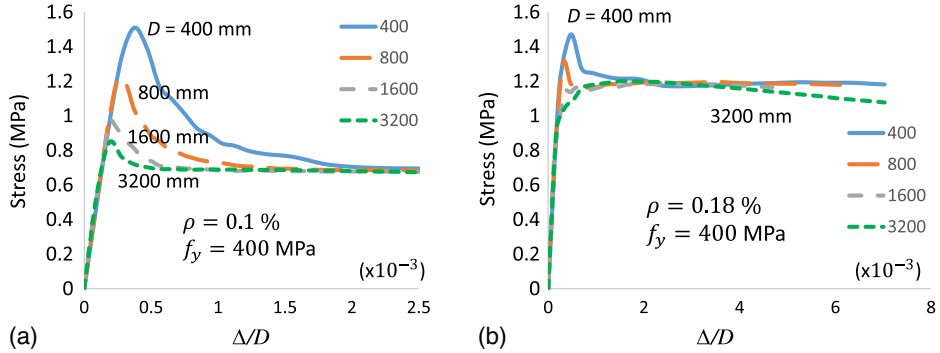

Fig. 4. Nominal stress versus relative displacement for three-point bend simulations of beams with (a) 0.10%; and (b) 0.18% reinforcement.

J. Eng. Mech., 2020, 146(10): 04020120

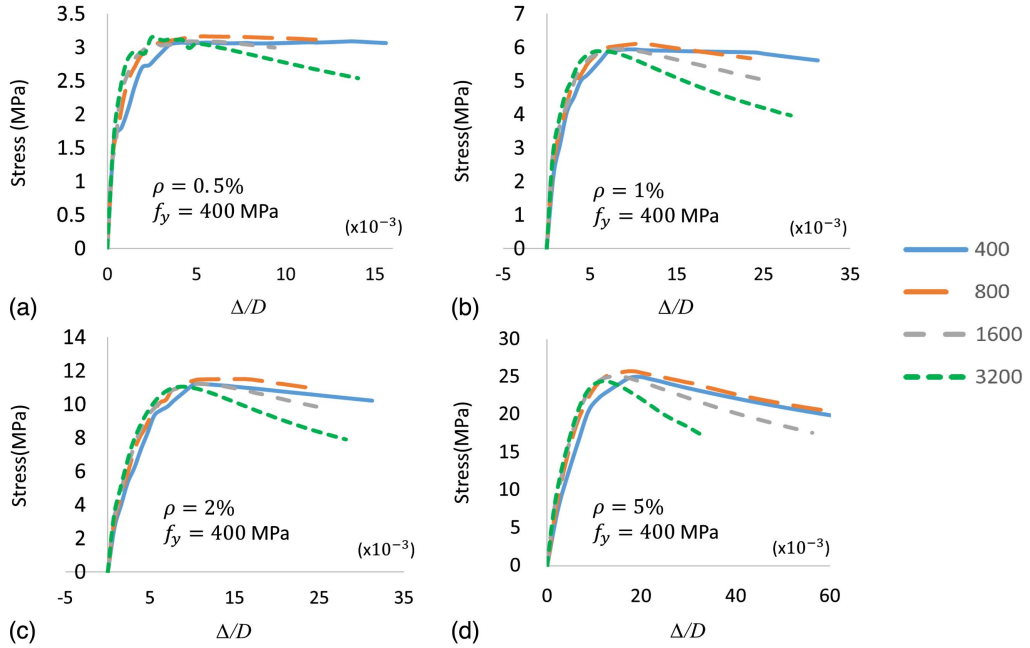

Fig. 6. Nominal stress versus relative displacement for three-point bend simulations of beams with (a) 0.5%; (b) 1%; (c) 2%; and (d) 5% reinforcement.

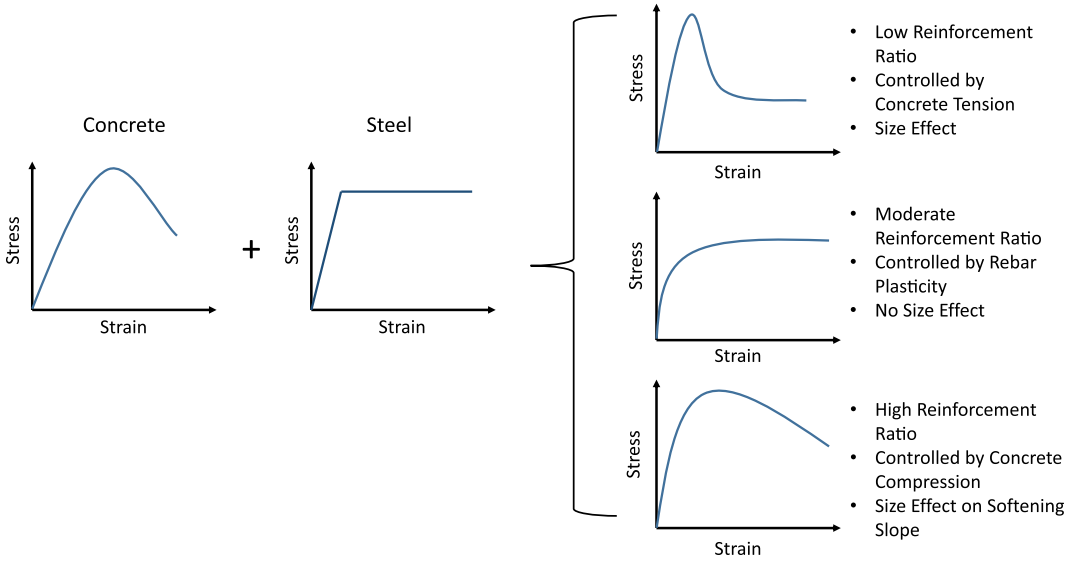

Fig. 7. Constitutive behavior of mesh-reinforced concrete.

softening seen on the curve for $D = 400$ mm would cause localization of cracking into a distinct crack. The maximum load is controlled by concrete for small sizes, and that is why the failure stress is the same for both cases. Fig. 9(b) shows how, at large sizes, the size effect curve depends on the yield limit of reinforcement.

The comparisons in Figs. 9(a and b) show that even for $\rho = 0.18\%$, one must expect distinct cracks to form in slabs of walls of larger sizes. Obviously, for low f_y and large D, it would be desirable to replace 0.18% with a formula for ρ as a function of both f_y and f_{te}, and ρ having the form

$$\rho_{\min} = \frac{f_{te}}{f_y} \tag{7}$$

where f_{te} = effective tensile strength of concrete which depends on D, due to the size effect. The requirement for the minimum of 0.18% is accurate only for normal concrete and yield limit $f_y = 413.7$ MPa (60,000 psi).

Conclusions

Based on the study carried out and the results obtained, the following conclusions can be drawn:

- Cracking localizes into larger cracks if and only if the size effect occurs. This is the premise of the present approach.

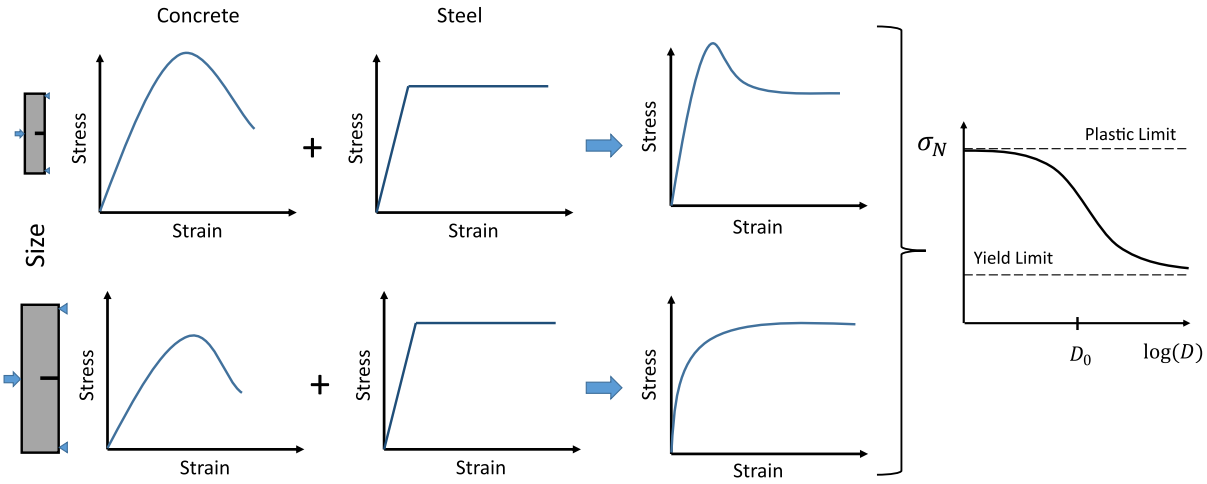

Fig. 8. Size effect of mesh-reinforced concrete.

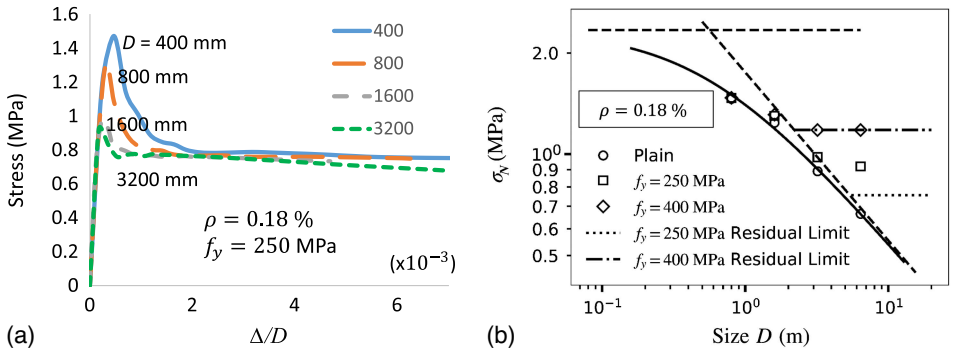

Fig. 9. Simulation results of 0.18% reinforced beams: (a) nominal stress versus relative displacement for three-point bend beams with 0.18% reinforcement ratio and $f_y = 250$ MPa; and (b) size effect plot for beams with 0.18% reinforcement.

- Quasibrittle fracture mechanics explains and supports the 92-year-old empirical requirement of ACI design code for minimum reinforcement ratio of concrete slabs and walls, called the shrinkage and temperature reinforcement, which is 0.18%.
- Fracture mechanics shows that weaker reinforcement cannot suppress the size effect with the accompanying formation of large localized cracks, and it cannot prevent postpeak softening.
- The minimum of 0.18% is only approximate. Knowing that the shrinkage and temperature reinforcement has a fracture mechanics justification validates the use of fracture mechanics to determine the minimum more precisely. The minimum reinforcement required for suppression of fracture and the size effect depends nonnegligibly on the steel yield limit, concrete strength, and fracture properties. It undoubtedly also depends on the loads applied in addition to shrinkage and temperature.
- The constitutive behavior of the homogenized steel–concrete composite with mesh reinforcement varies strongly with the reinforcement ratio. The concrete controls the fracture behavior of this composite only for low enough reinforcement ratios.
- The size effect can be avoided only if, for the same cross-section area, the tensile strength of yielding reinforcement exceeds the tensile strength of concrete.

Appendix I. Brief Review of Previous Studies

Previous theoretical studies (Shehata et al. 2003) generally did not consider the quasibrittle fracture and size effect. Baluch et al. (1992) proposed an expression to predict the minimum flexural reinforcement to avoid unstable crack propagation. Rao et al. (2008) documented that the beam size and flexural reinforcement percentage matter, and also concluded that the necessary minimum percentage of flexural steel reinforcement is inversely proportional to the beam depth. Fayyad and Lees (2015) reached similar conclusions. Ozbolt and Bruckner (1999) conducted numerical studies of reinforced concrete beams of different sizes and concluded that the requirement on the minimum reinforcement depends on the beam size as well as the material properties.

Rao et al. (2008) showed that the minimum reinforcement ensures ductility of concrete structures. As documented by Rasoolinejad and Bažant (2019), ductile response is controlled by steel and does not show a size effect. For example, in a study by Ghorbani-Renani et al. (2009), the walls exhibited ductile behavior and no size effect, whereas in another study by Maier and Thürlimann (1985), walls showed nonductile behavior for which a size effect must be expected (Rasoolinejad and Bažant 2019). During the Canterbury earthquake, some reinforced concrete walls formed a single crack in the plastic hinge region as opposed to distributed cracking (Henry 2013), which indicated lack of proper reinforcement of the wall.

Determining the minimum reinforcement ratio is critical for the design of concrete pavements (McCullough et al. 1976). Pavements are continuously under environmental stress, and minimum thermal and shrinkage reinforcement ensures ductile behavior and suppresses crack localization. This reinforcement is usually provided

J. Eng. Mech., 2020, 146(10): 04020120

by a steel mesh inside the concrete slab. In the case in which fiber-reinforced concrete (FRC) is used, the size effect exists but it may depend on the fiber type and geometry (Bažant et al. 2019).

Appendix II. Explanation and Advantages of Microplane Model

In this model, the microplane strains are assumed to be the projection of the continuum strain tensor. In an explicit algorithm, a vectorial constitutive law is used to calculate the stress vectors from the strain vectors on each microplane, which represents a kinematic constraint. The stress vectors are then used in the principle of virtual work to obtain the continuum stress tensor at each integration point of finite element. The idea of expressing the constitutive law in terms of vectors instead of tensors was first introduced by Taylor (1938) for the plastic (nonsoftening) polycrystalline metals. It was refined by Batdorf and Budiansky (1949) and others, and has been used until today in the so-called Taylor models for metals, in which microplane stress (rather than strain) vectors are calculated from the continuum stress tensor. This represents a static rather than kinematic constraint. However, in 1983, it was found at Northwestern that for softening damage, the static constraint must be replaced by a kinematic constraint (cf. Caner and Bažant 2012a). This led to microplane models for concrete, soils, rock, and composites, among others. The microplane model has five main advantages over the classical tensorial models such as Mohr-Coulomb or Drucker-Prager:

1. The vectorial, rather than tensorial, form of the microplane constitutive model has the advantage that constitutive behavior can be directly related to tensile crack opening, compression splitting, and frictional dilatant slip.
2. In tensorial constitutive laws, internal friction is expressed vaguely as a relation between the first stress invariant and second deviator invariant. In reality, the frictional slip happens only on one or two planes of distinct orientations, which is reproduced by the microplane model. Consequently, in the microplane model, the dilatancy ratio can be different from the friction coefficient without violating thermodynamic restrictions, and thus there is no need for nonassociated tensorial plasticity models violating thermodynamics, which lead to convergence loss (the microplane model is perfectly robust in computations).
3. A big practical advantage is that the microplane model can capture the vertex effect, e.g., the fact that a shear-stress increment that is superposed on large uniaxial compression and is parallel to the loading surface in the stress space has an incremental stiffness much softer than elastic (even three times lower for concrete), whereas all the classical tensorial models, such as, Mohr-Coulomb, Drucker-Prager, von Mises, as well as the models currently in commercial software such as ABAQUS, give, incorrectly, the elastic incremental stiffness.
4. As another advantage, the microplane model captures the fact that for hydrostatic compression, as well as uniaxial compressive strain, no strength limit and no postpeak softening exist, whereas in lesser confinement, it does.
5. A further advantage is correct modeling of hysteretic loops, response to cyclic loading, and subcritical fatigue crack propagation up to several thousand cycles (in agreement with Paris law).

An early objection to the microplane model was its computational demands. Indeed, for a system of 10 finite elements, the microplane model may run 10 times longer than a tensorial constitutive law. But for a system of 10 million finite elements, routinely used today, the difference in running time is <1% because the computer time increases only linearly with the constitutive law but quadratically with the number of unknowns.

Appendix III. Alternative Calculation of Minimum Reinforcement from Tolerable Crack Opening Width

Consider a macrocrack in an infinite slab of unit thickness subjected to remote uniaxial or biaxial tension σ_N. The length of open crack, $2a_0$, is considered as variable. The half-length of the FPZ at the crack front is c_f, and the length of the equivalent LEFM crack is $2a$, where $a = a_0 + c_f$. Because concrete undergoes distributed through-thickness cracking, its stress may be taken equal to its tensile strength, f_t, which means one neglects the postpeak softening in concrete. Equating σ_N^2, expressed from the size effect law, to σ_N^2, expressed from the sum of stresses in concrete and steel, yields the following condition:

$$\frac{E_{ef}G_f}{k(a_0+c_f)} = (f_t + \rho\sigma_s)^2, \quad \sigma_s = \min(f_y, f_s) \tag{8}$$

$$\text{where } E_{ef} = E_c + \rho E_s, \qquad f_s = E_s\bar{\varepsilon}_s, \qquad \bar{\varepsilon}_s = w_c/l_0 \tag{9}$$

where a_0, being the only length present, plays the role of structure size D; k = constant characterizing the structure shape, where for the case of infinite space, $k = \pi$, which is derived from the fact that for LEFM, the stress intensity factor is $K_I = \sigma\sqrt{\pi a}$; $\bar{\varepsilon}_s$ = average strain in steel bars crossing the cracks; f_y and f_s = yield and elastic stresses in steel; the command min is used to decide whether the steel is elastic or yielding; l_0 = length of the embedded steel bar segments along which the bars slip against concrete; and w_c = average crack width, which can be approximated from the asymptotic near-tip field of a LEFM crack

$$w_c = \sqrt{32/\pi}K_{I,ef}a_0/E_{ef}, \qquad K_{I,ef} = \sqrt{E_{ef}G_f} - K_{I,s},$$
$$K_{I,s} = \sigma_s\sqrt{\pi a_0} \tag{10}$$

where $K_{I,s}$ = stress intensity factor due to stress σ_s in steel approximately treated as a uniform closing pressure acting on the concrete crack faces.

The objective is to calculate the reinforcement ratio for which the crack width would not exceed a specified value, e.g., w_c = 0.2 mm. The values of E_c, f_t, E_s, f_y, G_f, and c_f must be given as the input. The problem is nonlinear and can be reduced to coupled quadratic equations with inequality constraint due to the min. The solution appears to be too complex to offer good insight.

Data Availability Statement

Some or all data, models, or code generated or used during the study are available in a repository online in accordance with funder data retention policies. Some or all data, models, or code that support the findings of this study are available from the corresponding author upon reasonable request.

The coding of M7, directly usable as a material subroutine in, e.g., VUMAT of ABAQUS, can be freely downloaded from Bažant's website: www.civil.northwestern.edu/people/bazant.

Acknowledgments

Partial funding under NSF Grant No. CMMI-2029641 to Northwestern University is gratefully appreciated.

References

ACI Committee. 2019. *Building code requirements for structural concrete (ACI 318-19) and commentary.* ACI 318-19. Farmington Hills, MI: ACI.

Baluch, M. H., A. K. Azad, and W. Ashmawi. 1992. "Fracture mechanics application to reinforced concrete members in flexure." In *Applications of fracture mechanics to reinforced concrete*, 413–436. London: Elsevier.

Batdorf, S. B., and B. Budiansky. 1949. *A mathematical theory of plasticity based on the concept of slip*. Technical Note No. 1871. Washington, DC: The National Aeronautics and Space Administration.

Bažant, Z. P. 1984. "Size effect in blunt fracture: Concrete, rock, metal." *J. Eng. Mech.* 110 (4): 518–535. https://doi.org/10.1061/(ASCE)0733-9399(1984)110:4(518).

Bažant, Z. P., and L. Cedolin. 2010. *Stability of structures: Elastic, inelastic, fracture and damage theories*. Singapore: World Scientific.

Bažant, Z. P., and R. Desmorat. 1994. "Size effect in fiber or bar pullout with interface softening slip." *J. Eng. Mech.* 120 (9): 1945–1962. https://doi.org/10.1061/(ASCE)0733-9399(1994)120:9(1945).

Bažant, Z. P., and M. Kazemi. 1990. "Determination of fracture energy, process zone longth and brittleness number from size effect, with application to rock and conerete." *Int. J. Fract.* 44 (2): 131. https://doi.org/10.1007/BF00047063.

Bažant, Z. P., and J. L. Le. 2017. *Probabilistic mechanics of quasibrittle structures: Strength, lifetime, and size effect*. Cambridge, UK: Cambridge University Press.

Bažant, Z. P., and B. H. Oh. 1983. "Crack band theory for fracture of concrete." *Matériaux et Constr.* 16 (3): 155–177. https://doi.org/10.1007/BF02486267.

Bažant, Z. P., and B. H. Oh. 1985. "Microplane model for progressive fracture of concrete and rock." *J. Eng. Mech.* 111 (4): 559–582. https://doi.org/10.1061/(ASCE)0733-9399(1985)111:4(559).

Bažant, Z. P., and J. Ozbolt. 1992. "Compression failure of quasibrittle material: Nonlocal microplane model." *J. Eng. Mech.* 118 (3): 540–556. https://doi.org/10.1061/(ASCE)0733-9399(1992)118:3(540).

Bažant, Z. P., and J. Planas. 1997. *Fracture and size effect in concrete and other quasibrittle materials*. London: CRC Press.

Bažant, Z. P., and P. C. Prat. 1988. "Microplane model for brittle-plastic material. I: Theory." *J. Eng. Mech.* 114 (10): 1672–1688. https://doi.org/10.1061/(ASCE)0733-9399(1988)114:10(1672).

Bažant, Z. P., M. Rasoolinejad, A. Dönmez, and W. Luo. 2019. "Dependence of fracture size effect and projectile penetration on fiber content of FRC." In *Proc., IOP Conf. Series: Materials Science and Engineering*, 012001. Bristol, UK: IOP Publishing.

Bažant, Z. P., S. Sener, and J.-K. Kim. 1987. "Effect of cracking on drying permeability and diffusivity of concrete." *ACI Mater. J.* 84 (5): 351–357.

Caner, F. C., and Z. P. Bažant. 2012a. "Microplane model M7 for plain concrete. I: Formulation." *J. Eng. Mech.* 139 (12): 1714–1723. https://doi.org/10.1061/(ASCE)EM.1943-7889.0000570.

Caner, F. C., and Z. P. Bažant. 2012b. "Microplane model M7 for plain concrete. II: Calibration and verification." *J. Eng. Mech.* 139 (12): 1724–1735. https://doi.org/10.1061/(ASCE)EM.1943-7889.0000571.

Di Luzio, G., and G. Cusatis. 2018. "Cohesive crack analysis of size effect for samples with blunt notches and generalized size effect curve for quasi-brittle materials." *Eng. Fract. Mech.* 204 (Dec): 15–28. https://doi.org/10.1016/j.engfracmech.2018.09.003.

England, G., and A. Ross. 1962. "Reinforced concrete under thermal gradients." *Mag. Concr. Res.* 14 (40): 5–12. https://doi.org/10.1680/macr.1962.14.40.5.

Fayyad, T. M., and J. M. Lees. 2015. "Evaluation of a minimum flexural reinforcement ratio using fracture-based modelling." In *Proc., IABSE Symp. Report*, 1–8. Zürich, Switzerland: International Association for Bridge and Structural Engineering.

Ghorbani-Renani, I., N. Velev, R. Tremblay, D. Palermo, B. Massicotte, and P. Léger. 2009. "Modeling and testing influence of scaling effects on inelastic response of shear walls." *ACI Struct. J.* 106 (3): 358.

Gilbert, R. I. 1992. "Shrinkage cracking in fully restrained concrete members." *Struct. J.* 89 (2): 141–149.

Henry, R. 2013. "Assessment of minimum vertical reinforcement limits for RC walls." *Bull. N. Z. Soc. Earthquake Eng.* 46 (2): 88–96. https://doi.org/10.5459/bnzsee.46.2.88-96.

Kianoush, M., M. Acarcan, and A. Ziari. 2008. "Behavior of base restrained reinforced concrete walls under volumetric change." *Eng. Struct.* 30 (6): 1526–1534. https://doi.org/10.1016/j.engstruct.2007.10.009.

Maier, J., and B. Thürlimann. 1985. "Bruchversuche an stahlbetonscheiben." *Bericht/Institut für Baustatik und Konstruktion ETH Zürich* 8003 (1): 29. https://doi.org/10.1007/978-3-0348-5190-9.

McCullough, B. F., A. Adou-Ayyash, W. R. Hudson, and J. P. Randall. 1976. *Design of continuously reinforced concrete pavements for highways*. NCHRP Research Results Digest. Washington, DC: Transportation Research Board.

Mertol, H. C., S. Rizkalla, P. Zia, and A. Mirmiran. 2010. "Creep and shrinkage behavior of high-strength concrete and minimum reinforcement ratio for bridge columns." *PCI J.* 55 (3): 1–3. https://doi.org/10.15554/pcij.06012010.138.154.

Ozbolt, J., and M. Bruckner. 1999. "Minimum reinforcement requirement for RC beams." *Eur. Struct. Integr. Soc.* 24: 181–201. https://doi.org/10.1016/S1566-1369(99)80069-7.

Rao, G. A., I. Vijayanand, and R. Eligehausen. 2008. "Studies on ductility and evaluation of minimum flexural reinforcement in RC beams." *Mater. Struct.* 41 (4): 759–771. https://doi.org/10.1617/s11527-007-9280-7.

Rasoolinejad, M., and Z. P. Bažant. 2019. "Size effect of squat shear walls extrapolated by microplane model M7." *ACI Struct. J.* 116 (3): 304–307. https://doi.org/10.14359/51714478.

Rasoolinejad, M., S. Rahimi-Aghdam, and Z. P. Bažant. 2019. "Prediction of autogenous shrinkage in concrete from material composition or strength calibrated by a large database, as update to model B4." *Mater. Struct.* 52 (2): 33. https://doi.org/10.1617/s11527-019-1331-3.

Shah, S. P., and C. Ouyang. 1991. "Mechanical behavior of fiber-reinforced cement-based composites." *J. Am. Ceram. Soc.* 74 (11): 2727–2953. https://doi.org/10.1111/j.1151-2916.1991.tb06836.x.

Shehata, I. A., L. C. Shehata, and S. L. Garcia. 2003. "Minimum steel ratios in reinforced concrete beams made of concrete with different strength—Theoretical approach." *Mater. Struct.* 36 (1): 3. https://doi.org/10.1007/BF02481565.

Sule, M., and K. Van Breugel. 2004. "The effect of reinforcement on early-age cracking due to autogenous shrinkage and thermal effects." *Cem. Concr. Compos.* 26 (5): 581–587. https://doi.org/10.1016/S0958-9465(03)00078-7.

Suprenant, B. A. 2002. "Shrinkage and temperature reinforcement." *ACI Concr. Int.* 24 (9): 72–76.

Taylor, G. I. 1938. "Plastic strain in metals." *J. Inst. Met.* 62: 307–324.

Wei, Y., S. Liang, W. Guo, and W. Hansen. 2017. "Stress prediction in very early-age concrete subject to restraint under varying temperature histories." *Cem. Concr. Compos.* 83 (Oct): 45–56. https://doi.org/10.1016/j.cemconcomp.2017.07.006.